


## Europium oxide: Growth guide for the first monolayers on oxidic substrates

Paul Rosenberger<sup>1,2</sup> and Martina Müller<sup>3,\*</sup>

<sup>1</sup>*Peter Grünberg Institut (PGI-6), Forschungszentrum Jülich, 52425 Jülich, Germany*

<sup>2</sup>*Fakultät Physik, Technische Universität Dortmund, 44221 Dortmund, Germany*

<sup>3</sup>*Fachbereich Physik, Universität Konstanz, 78457 Konstanz, Germany*

 (Received 10 December 2021; revised 10 February 2022; accepted 14 March 2022; published 11 April 2022)

Interfacial oxygen exchange at oxide interfaces bears huge potential in stabilizing metastable or novel phases of functional oxides down to the monolayer limit. By taking advantage of active oxygen supply of the substrate material, waiving any external oxygen dosage, high-quality, crystalline ultrathin films of the Heisenberg ferromagnet europium monoxide (EuO) were stabilized on YSZ (001). This so-called redox-assisted growth mode (or, vice versa, the extreme case of a distillation growth) was monitored end to end by *in situ* x-ray photoelectron emission spectroscopy and electron diffraction techniques. The evolution of Eu 3*d* core levels allows us to disentangle the processes of interfacial oxygen diffusion and vacancy formation in stabilizing the very first monolayers of EuO on YSZ (001). An expedient background correction analysis is presented, which allows us to quantify the critical  $\text{Eu}^{3+}/\text{Eu}^{2+}$  ratio in the ultrathin film regime. We concluded on the key mechanisms of redox-assisted EuO/YSZ (001) thin film synthesis, which merge in a universal three-process growth model that may serve as guideline for redox-assisted synthesis of metastable low-dimensional oxides.

DOI: [10.1103/PhysRevMaterials.6.044404](https://doi.org/10.1103/PhysRevMaterials.6.044404)

### I. INTRODUCTION

Oxide interfaces exhibit a large variety of technologically relevant functionalities [1,2]. They give rise to the emergence of quantum phenomena such as the well-known two-dimensional electron gas (2DEG), originally observed at the SrTiO<sub>3</sub>/LaAlO<sub>3</sub> interface [3]. Consequently, controlling the underlying interfacial processes opens up the possibility to tailor and tune functionalities of oxide interfaces. Oxygen diffusion has been shown to be a key process taking place already during sample growth and results in novel functionalities [4–8]. For example, interfacing the semiconducting 4*f* Heisenberg ferromagnet europium monoxide (EuO) with selected oxides by molecular beam epitaxy (MBE) allows us to control oxygen diffusion and may reveal a large variety of coupled quantum phenomena [9,10]. A recent example is the formation of a 2DEG at the magnetically tunable EuO/SrTiO<sub>3</sub> interface, resulting from an interfacial redox reaction [11]. This process makes use of the high reactivity of europium and the thermodynamically favored formation of EuO on the cost of reducing Ti<sup>4+</sup> in STO. On the other hand, oxygen diffusion may act detrimentally on the control of interfaces because stoichiometries can be affected in an undesired way, hindering, e.g., the stabilization of strained overlayers.

EuO grown on yttria-stabilized zirconia (YSZ) typically serves as a reference system for ultrathin EuO films as the lattice constant of YSZ ranges from 5.138–5.142 Å for 9.0 mol% Y<sub>2</sub>O<sub>3</sub> and 10.0 mol% Y<sub>2</sub>O<sub>3</sub> [12], respectively, which almost perfectly matches that of EuO (5.142 Å [13]). In this study we use 9.5 mol% Y<sub>2</sub>O<sub>3</sub>. Furthermore, YSZ

and EuO are considered to be chemically stable in contact with each other. Hence, several approaches of synthesizing EuO/YSZ (001) using MBE have been pursued [14–18]. Perfect stoichiometry and layer-by-layer growth are reported for a growth temperature of 400 °C in the adsorption-limited growth mode [15,16], while the ability to reduce the growth temperature of epitaxial EuO was accomplished by inserting an MgO buffer layer [19]. Both mention the general ability of YSZ to supply oxygen to form the EuO film. This oxygen supply is also discussed in a further study, in which the aim of growing oxygen-deficient EuO<sub>1-x</sub> films failed due to oxygen diffusion [20]. However, the interface formation of the EuO/YSZ (001) model system had not yet been studied down to the single monolayer level. Only Lömker *et al.* found indications for an interfacial overoxidation of EuO/YSZ (001) for a deposition temperature of  $T_S = 500$  °C [21]. In the present study, we investigate the oxygen diffusion and its consequences for the interface formation (i.e., the very first monolayers) of EuO and its model substrate YSZ. We interpret the findings and derived a three-process growth model of EuO/YSZ (001), which may serve as a guide for the monolayer-controlled synthesis of the Heisenberg model system EuO on oxidic substrates.

### II. EXPERIMENTAL DETAILS

#### Setup and methods

Using MBE, EuO films were synthesized on YSZ (001) substrates (Crystec GmbH). The substrates were annealed *in situ* in an oxygen atmosphere for 2 h at  $T_S = 600$  °C.

Eu metal was evaporated from a Knudsen cell. The base pressure of the chamber was  $p_{\text{MBE}} \leq 2 \times 10^{-10}$  mbar. The Eu deposition rate of  $r_{\text{Eu}} = 0.13$  Å/s and was measured

\*martina.mueller@uni-konstanz.de

using a quartz crystal microbalance. We mainly synthesized films at a substrate temperature  $T_S = 400^\circ\text{C}$ . Synthesis was performed without supplying oxygen to the chamber, i.e., the extreme case of the distillation (or adsorption-limited) growth mode.

RHEED and LEED patterns were taken using a SPECS RHD-30 and ErLEED-1000, respectively, in order to study the crystalline quality of the films. The samples' stoichiometry as well as their thickness was determined by *in situ* x-ray photoelectron spectroscopy (XPS) with nonmonochromatized Al  $K_\alpha$  radiation. A setup consisting of a SPECS XR-50 x-ray source and a SPECS Phoibos 100 analyzer was used.

### III. ANALYSIS OF XPS DATA

#### A. Quantification of $\text{Eu}^{3+}$ ratio

The aforementioned properties of europium oxide are solely present in metastable  $\text{EuO}$ , i.e., the pure  $\text{Eu}^{2+}$  state of  $\text{Eu}$ . However, due to the high reactivity of  $\text{Eu}$  the undesired formation of a certain ratio of  $\text{Eu}^{3+}$  in thus mixed-valent films is a well-known issue to be resolved. Hence, understanding its origin and confirming the exact stoichiometry of  $\text{EuO}$  thin films is essential. Therefore, the  $\text{Eu}^{3+}$  ratio of a series of mixed-valent films needs to be analyzed and quantified in a comparable and efficient manner. In the following, an approach for such a straightforward method is introduced. The basic idea is to simulate the measured spectra using background-corrected spectra of pure  $\text{Eu}^{2+}$  and pure  $\text{Eu}^{3+}$ . For this, the pure spectra are added up with a weighting factor  $\xi$ :

$$I_{\text{total}}(\xi, E) = \xi I_{\text{Eu}^{3+}}(E) + (1 - \xi) I_{\text{Eu}^{2+}}(E). \quad (1)$$

$\xi$  then denotes the ratio of photoelectrons originating from  $\text{Eu}^{3+}$  ions contributing to the spectrum and, hence, the ratio of  $\text{Eu}^{3+}$  in the film.

We use the  $\text{Eu } 3d_{5/2}$  core level for quantitative analysis as it has a high Al  $K_\alpha$  cross section and is very sensitive to tiny changes in the  $\text{Eu}^{3+}$  contribution. All spectra were shifted in energy such that the peak positions match the reported ones [22]:  $E_{\text{bin}}(\text{Eu}^{2+}) = 1124.9 \text{ eV}$  and  $E_{\text{bin}}(\text{Eu}^{3+}) = 1134.7 \text{ eV}$ .

Both pure  $\text{Eu}$  spectra, see Fig. 1, were indeed taken from the same sample: the  $\text{Eu}^{2+}$  spectrum (green) after synthesizing a stoichiometric film in the adsorption limited growth mode, and the  $\text{Eu}^{3+}$  spectrum (red) after annealing this stoichiometric  $\text{EuO}$  film in an oxygen atmosphere. For inelastic background correction, we use Shirley-type backgrounds in the binding energy ranges 1110–1138 eV ( $\text{Eu}^{2+}$ ) and 1110–1147.5 eV ( $\text{Eu}^{3+}$ ). While a single Shirley background would work for the  $\text{Eu}^{2+}$  spectrum, it would cut the data around the minimum at 1140.6 eV in case of  $\text{Eu}^{3+}$ , which is nonphysical. Hence, we split the energy ranges and construct a Shirley-type background for each of the pure spectra out of two separate Shirley backgrounds. Therefore, we consider the binding energy range  $E_A$  to  $E_C$  for  $\text{Eu}^{2+}$  ( $E_{A'}$  to  $E_{C'}$  for  $\text{Eu}^{3+}$ ) and choose an intermediate binding energy  $E_B$  ( $E_{B'}$ ), which is the position of the local minimum on the high binding energy side next to the main peak. All binding energy values are given in Fig. 1. Here, we describe the procedure for  $\text{Eu}^{2+}$ ; for  $\text{Eu}^{3+}$  replace A, B, and C by  $A'$ ,  $B'$ , and  $C'$ , respectively.

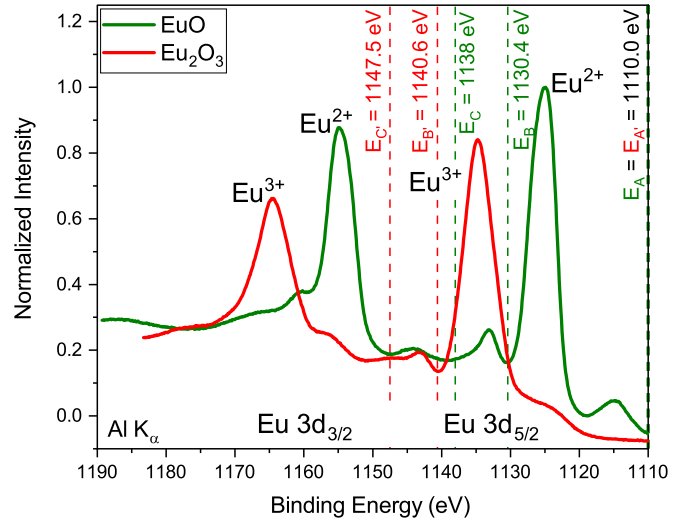


FIG. 1. XPS spectra of the  $\text{Eu } 3d$  core level taken from a stoichiometric  $\text{EuO}$  film, i.e., pure  $\text{Eu}^{2+}$  (green) and an  $\text{Eu}_2\text{O}_3$  film, i.e., pure  $\text{Eu}^{3+}$  (red). Vertical dashed lines display the binding energy values used for constructing the Shirley-type background.

We then define a Shirley background  $b_{AB}$  from  $E_A$  to  $E_B$  and a second one from  $E_B$  to  $E_C$ . To fulfill the boundary conditions (i)  $b_{AB}(E_A) = I_0(E_A)$ , (ii)  $b_{AB}(E_B) = b_{BC}(E_B)$ , and (iii)  $b_{BC}(E_C) = I_0(E_C)$ , where  $I_0(E)$  is the intensity before background subtraction, we scale the two backgrounds as follows:

$$b(E) = \begin{cases} k \cdot (b_{AB}(E) - b_{AB}(E_A)) + b_{AB}(E_A); & E \leq E_B \\ k \cdot [\alpha \cdot (b_{BC}(E) - b_{BC}(E_B))] + b_{BC}(E_B); & E > E_B. \end{cases} \quad (2)$$

The parameter  $\alpha$  defines the relative scaling of the two background sections, while  $k$  is defined such that boundary conditions (i) and (iii) are fulfilled. Both parameters may be different for the  $\text{Eu}^{2+}$  and  $\text{Eu}^{3+}$  spectrum.

For a proper choice of  $\alpha$  (and, thus,  $k$ ), further spectral information is needed. According to theoretical calculations by Cho *et al.*, the  $\text{Eu}^{2+}$  satellite's intensity is 10% of the main peak's intensity [23]. We thus vary  $\alpha$  such that this condition is fulfilled to a good approximation. The resulting background and background-corrected spectrum are shown in Fig. 2(a). In a next step, the parameters have to be determined for the  $\text{Eu}^{3+}$  spectrum. We take advantage of the fact that both pure spectra were taken from the same sample before and after oxidizing it. Hence, we know that the same number of  $\text{Eu}$  atoms contributes to both spectra. It is therefore justified to assume that the integrals over both  $\text{Eu } 3d_{5/2}$  spectra have to be identical, i.e.,

$$\int_{E_{A'}}^{E_{C'}} I_{\text{Eu}^{2+}}(E) dE \stackrel{!}{=} \int_{E_A}^{E_C} I_{\text{Eu}^{3+}}(E) dE. \quad (3)$$

$\alpha$  is now determined such that this condition is fulfilled. The resulting background and background-corrected spectrum are shown in Fig. 2(b).

The so-obtained spectra and backgrounds are now used to simultaneously perform a background correction of the spectra and fitting the background-corrected spectra. For this

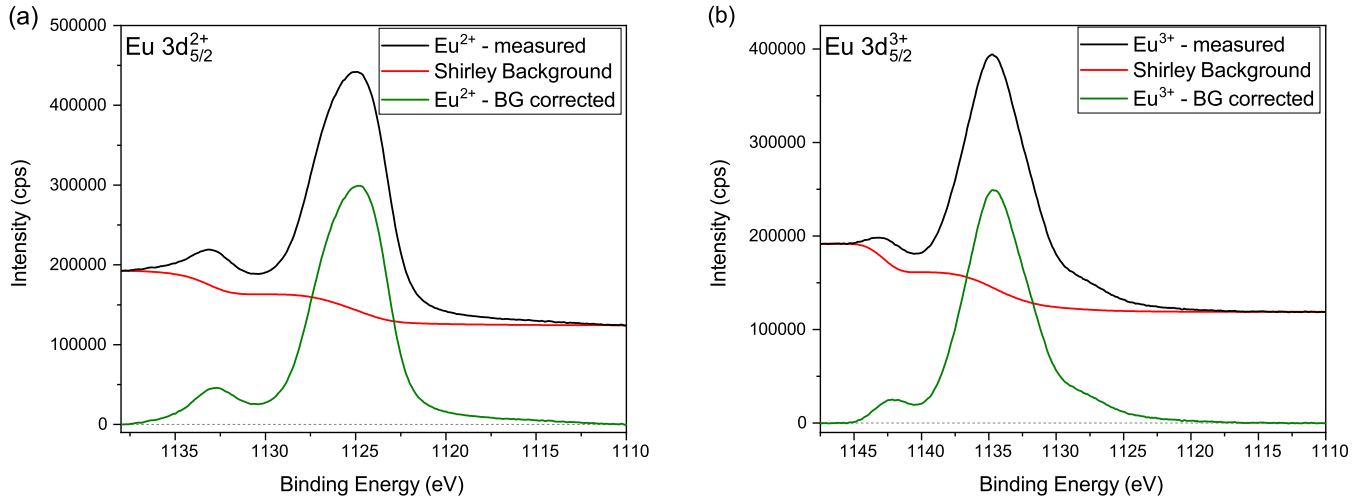


FIG. 2. Measured (reference) spectra (black), background (red) and background-corrected spectra (green) of the  $\text{Eu } 3d_{5/2}$  core levels of (a) pure  $\text{Eu}^{2+}$  and (b) pure  $\text{Eu}^{3+}$  valencies.

purpose, we assume that not only the background-corrected measured spectra can be fitted according to Eq. (1), but that also the backgrounds of the pure spectra contribute to that of a mixed-valent film with the weighting  $\xi$ ,

$$b_{\text{total}}(\xi, E) = h \cdot [\xi b_{\text{Eu}^{3+}}(E) + (1 - \xi) b_{\text{Eu}^{2+}}(E)]. \quad (4)$$

The scaling factor  $h$  ensures that spectrum and background match each other at  $E_A$  and  $E_C$ . Hence,  $\xi$  is the only free parameter in the fitting process. For a chosen  $\xi$ , the background according to Eq. (4) is subtracted from the measured spectrum. The resulting background-corrected spectrum is then plotted together with the spectrum calculated using Eq. (1). By varying  $\xi$ , this process is iterated until the spectra match most appropriately. An example of a film containing 46%  $\text{Eu}^{3+}$  is shown in Fig. 3. We estimate that the error is as low as  $\Delta\xi \approx 0.02$ .

### B. Determination of the $\text{EuO}$ film thickness

We use the attenuation of the  $\text{Zr } 3d_{5/2}$  signal to determine the thickness  $d$  of the overlying  $\text{EuO}_x$  films by XPS, i.e.,

$$d = -\lambda \ln \left( \frac{A_{\text{Zr } 3d}(d)}{A_{\text{Zr } 3d}(0)} \right) \cdot \cos(\Theta). \quad (5)$$

$A_{\text{Zr } 3d}(0)$  and  $A_{\text{Zr } 3d}(d)$  are the (background-corrected)  $\text{Zr } 3d_{5/2}$  intensities before and after the deposition of an  $\text{EuO}_x$  film, respectively. The angle  $\Theta$  denotes the deviation from a normal emission geometry (here  $\Theta = 15^\circ$ ).  $\lambda$  is the effective attenuation length (EAL) in  $\text{EuO}$  of the photoelectrons excited from the  $\text{Zr } 3d$  core level. It was calculated according to Jablonski and Powell [24] using the inelastic mean-free path (IMFP) and the transport mean-free path (TRMFP) obtained from SESSA 2.0 [25]. Taking into account the film roughness and the deposited amount of  $\text{Eu}$  metal, we assume the error to be  $\Delta d = 0.1 \text{ nm}$ .

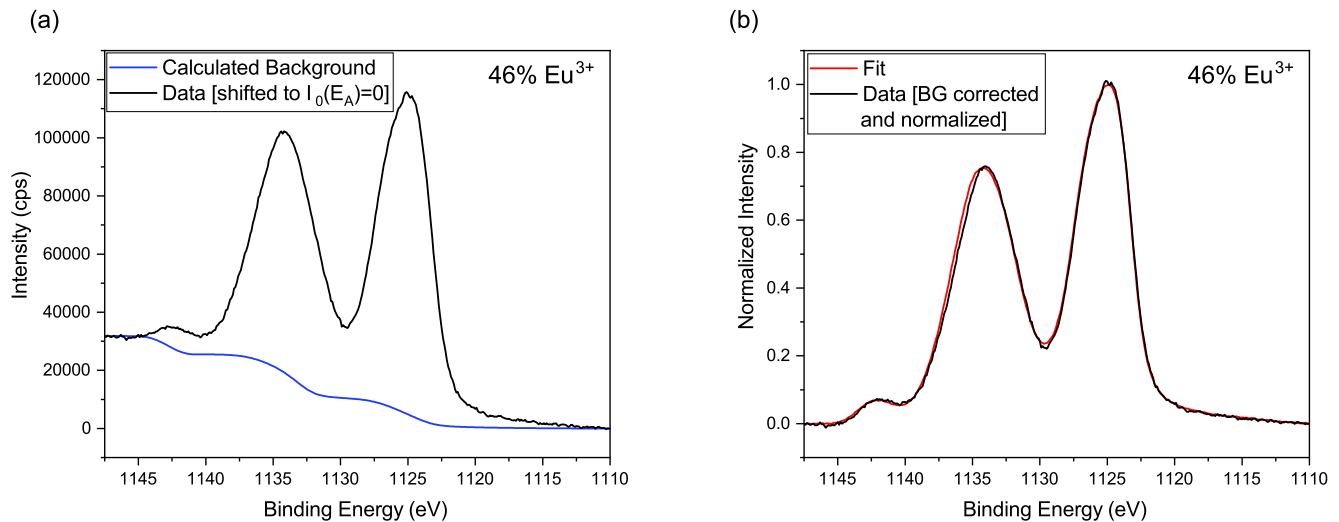


FIG. 3. Fit results for a sample containing 46%  $\text{Eu}^{3+}$ : (a) Measured spectrum (black) and background according to Eq. (4) (blue). (b) Background-corrected spectrum (black) and fit according to Eq. (1) (red).

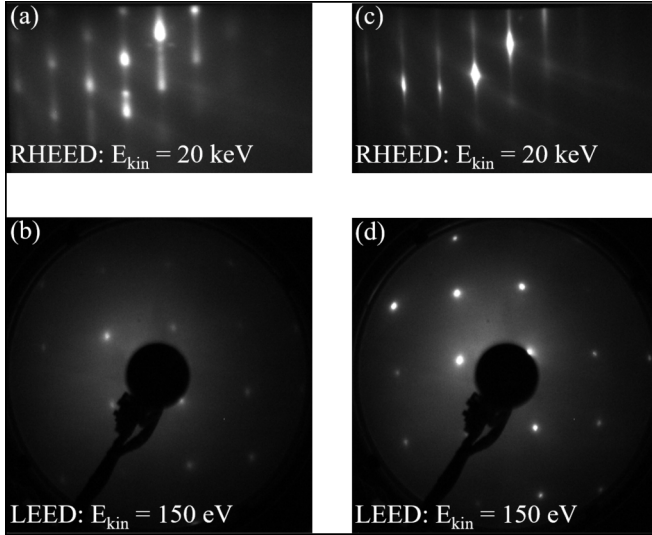


FIG. 4. RHEED (top) and LEED (bottom) patterns of films synthesized without (left) and with (right) externally supplied oxygen. The deposition time was 1 h for the bulklike film with externally supplied oxygen and 30 min for the thin film without oxygen supply. The LEED patterns exhibit the expected fourfold symmetry of the EuO (001) surface. The RHEED patterns imply that synthesis without oxygen supply might lead to a higher roughness.

## IV. RESULTS

### A. Interfacial overoxidation

#### 1. Surface structure analysis by RHEED/LEED

In Fig. 4, RHEED and LEED patterns of a EuO film synthesized without (w/o), Figs. 4(a), 4(b), and with (w/) external oxygen supply, Figs. 4(c), 4(d), are shown. The film synthesized w/O<sub>2</sub> has been synthesized for  $t_{\text{Eu}} = 1$  h and its thickness is estimated as  $d > 15$  nm. The corresponding RHEED pattern shown in Fig. 4(c) shows streaks with a slight tendency towards multiple reflexes, indicating a surface with terraces. The corresponding LEED pattern shows sharp spots in the fourfold rotational symmetry, as expected for a well-oriented film of cubic EuO (001).

The EuO film synthesized w/o O<sub>2</sub> was grown by supplying europium metal onto the YSZ substrate kept at  $T = 400$  °C for  $t_{\text{Eu}} = 30$  min. We estimate a film thickness of  $d = 2.9 \pm 0.1$  nm. The RHEED pattern, Fig. 4(a), shows multiple spots, indicating island growth and a rougher surface compared to the EuO film synthesized w/O<sub>2</sub>. The LEED pattern, Fig. 4(b), however, reflects the expected fourfold rotational symmetry of cubic EuO (001). We thus state that the crystalline quality of EuO synthesized w/o external O<sub>2</sub> supply is good, although the film roughness is high compared to the classical distillation w/O<sub>2</sub>.

#### 2. Chemical analysis by XPS

Using XPS, we studied the stoichiometry of EuO/YSZ (001) films synthesized without supplying O<sub>2</sub> and under UHV conditions. This means that all oxygen in the EuO film must originate from the YSZ substrate. The substrate temperature was set to  $T_S = 400$  °C, and we varied the deposition time  $t_{\text{Eu}}$  between one and 40 min. As can be

seen from the XPS spectra shown in Fig. 5(a), we find a perfectly stoichiometric EuO film for  $t_{\text{Eu}} = 40$  min, while for  $t_{\text{Eu}} = 1$  min, we find a pronounced Eu<sup>3+</sup> feature in addition. This finding underlines that oxygen from the YSZ substrate causes the formation of Eu<sup>3+</sup>, i.e., an overoxidized layer, at the interface. This is, however, in contrast to an earlier report by Sutarto *et al.* [15], who claimed that EuO/YSZ grows perfectly free from Eu<sup>3+</sup> when using the classical distillation growth mode.

Next, we quantified the Eu<sup>3+</sup> ratio in the EuO films as described in Sec. III A and determined the film thickness  $d$  using Eq. (5). In Fig. 5(b), the EuO film thickness  $d$  is plotted as a function of the deposition time  $t_{\text{Eu}}$ . For  $t_{\text{Eu}} < 5$  min, we find a quasi linear behavior of  $d(t_{\text{Eu}})$ . Surprisingly, for  $t_{\text{Eu}} = 5$  min and  $t_{\text{Eu}} = 30/40$  min, the EuO film thicknesses are comparable. We thus conclude, that the oxygen supply from the YSZ substrate is self-limiting and the EuO film thickness saturates for a critical  $t_{\text{Eu}}$ . Without external oxygen supply, we find the maximum obtainable thickness of EuO/YSZ (001) films at  $T_S = 400$  °C as  $d_{\text{max}} < 3$  nm. This self-limitation may be caused by two different effects, (i) a limited reducibility of the YSZ substrate and, thus, a finite oxygen reservoir, and (ii) the fact that the grown EuO film itself acts as a diffusion barrier for the oxygen provided by the underlying substrate.

In Fig. 6, the content  $\xi$  (in %) of Eu<sup>3+</sup> in the film as a function of the film thickness  $d$  is shown, and we observe a strong decrease of  $\xi$  with increasing  $d$ . Surprisingly, although we found the films synthesized for  $t_{\text{Eu}} = 5$  min and  $t_{\text{Eu}} = 30/40$  min to be of similar thickness, we find that only the latter ones contain a negligible ratio of Eu<sup>3+</sup>.

In order to explain the thickness dependence of the observed Eu<sup>3+</sup> content by a stacking of differently oxidized layers, we used several models of buried overoxidized interface layers to simulate the contribution of Eu<sup>3+</sup> to the XPS spectra. For that, we assumed a layer-by-layer structure and an EuO monolayer (ML) thickness of 2.571 Å [13]. In Fig. 6, we compare four such models with the stacking sequences of layers containing a given percentage of Eu<sup>3+</sup> as shown in Table I.

We find that models 2 and 3 match the data best within the error bars, while models 1 and 4 underestimate or rather overestimate the Eu<sup>3+</sup> content, in particular for monolayer thin films. Hence, those layer stackings might explain the observed dependency between the Eu<sup>3+</sup>-related XPS signal and the film thickness. However, another possible explanation

TABLE I. Models of the EuO<sub>x</sub>/YSZ interface chemistry with different layer stackings. Numbers display the percentage of Eu<sup>3+</sup> relative to the total amount of Eu ions (i.e., Eu<sup>2+</sup> plus Eu<sup>3+</sup>). The Eu<sup>3+</sup>-related XPS signal is plotted in Fig. 6.

Layer	Model 1	Model 2	Model 3	Model 4
n <sup>th</sup> ML; n ≥ 3	0%	0%	0%	0%
2 <sup>nd</sup> ML	0%	66.67%	66.67%	100%
1 <sup>st</sup> ML	100%	66.67%	100%	100%
Substrate	YSZ	YSZ	YSZ	YSZ



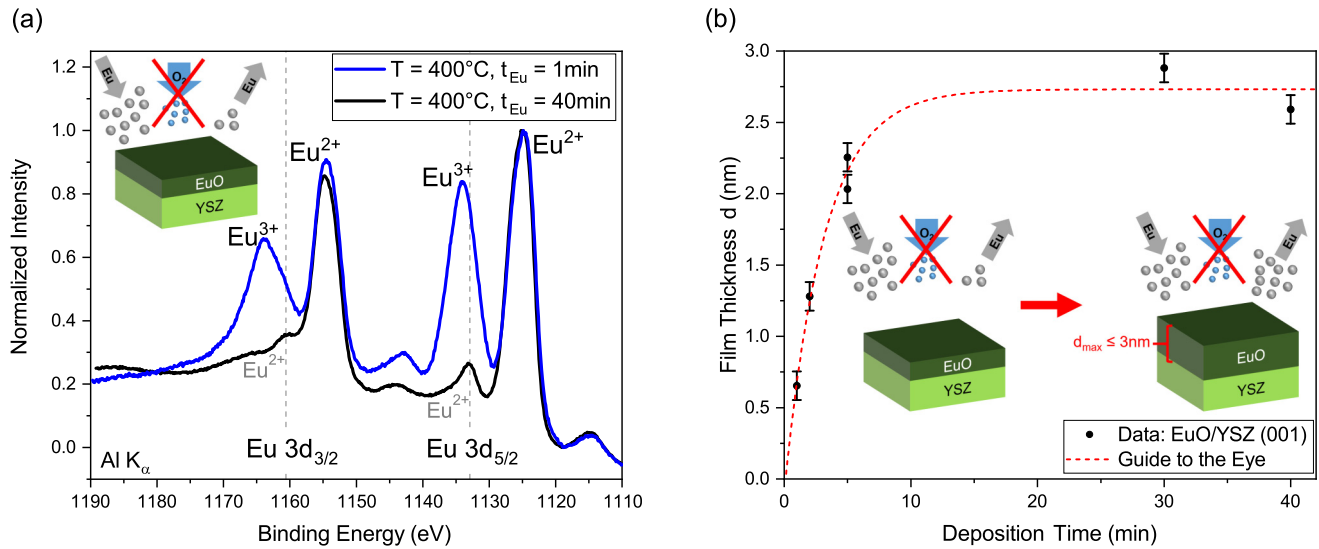


FIG. 5. (a) Normalized XPS spectra of the Eu  $3d_{5/2}$  core level of films synthesized by supplying Eu metal only for 1 min (black) and 40 min (blue). (b) EuO film thickness  $d$  as function of the Eu deposition time  $t$  and w/o  $O_2$ . While linear increase is observed for  $t_{Eu} < 5$  min, a saturation of the EuO film thickness sets in for  $t_{Eu} > 5$  min. The red dashed line serves as a guide to the eye.

is a continuous reduction of initially overoxidized films upon ongoing Eu deposition, if Eu metal and  $Eu^{3+}$ -rich phases undergo a redox reaction to form stoichiometric EuO. This will be discussed below.

In summary, we found that oxygen originating from the YSZ substrate causes an interfacial overoxidation of the EuO film even in the extreme distillation regime. The observed  $Eu^{3+}$  content decreases with increasing EuO film thickness and approaches zero for  $t_{Eu} > 5$  min. This decrease in the XPS signal might be caused by either overoxidized layers at the film/substrate interface that are covered by stoichiometric EuO or a continuous reduction of the initially strongly overoxidized layers at the interface.

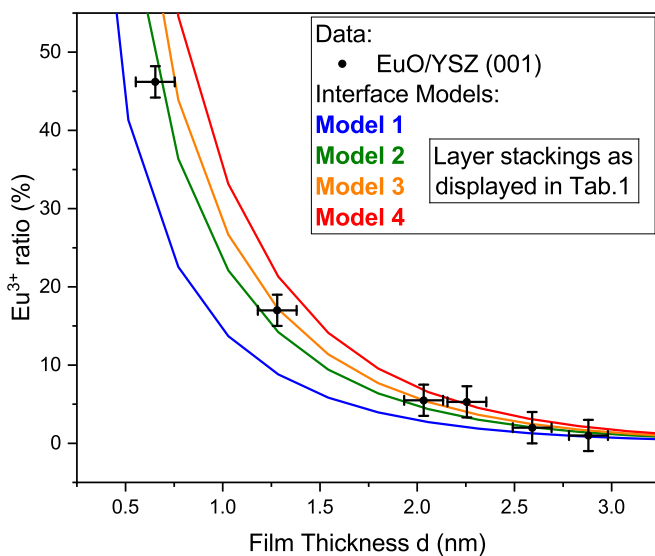
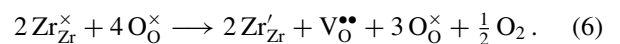


FIG. 6.  $Eu^{3+}$  ratio as function of the film thickness  $d$  of films synthesized without oxygen supply. Two models, 2 and 3, (colored lines) of a buried, stably overoxidized interface (as introduced in Table I) fit the data within the error bars.

## B. Role of oxygen vacancies in YSZ

We found that YSZ substrates supply oxygen causing the formation of  $Eu^{3+}$  even if no oxygen is supplied externally, i.e., under extreme distillation conditions. From thermodynamic considerations as displayed in the corresponding Ellingham diagram, a reduction of  $ZrO_2$ , which is the main ingredient of YSZ, in favor of further oxidation of EuO is not expected [14]. However, this model is only valid for the complete reduction/oxidation of metals with structural phase transition. It is, thus, not valid for the formation of a thin film on a thick substrate. Here, the substrate is only slightly reduced so that we have to deal with vacancies instead of complete reduction, i.e., in Kröger-Vink notation [26],



The oxygen ion conductivity of YSZ is known to be strongly temperature dependent [27] and at  $T_S = 400^\circ C$  already large compared, e.g., to that of  $LaAlO_3$  [28]. It is thus intuitive to explain the YSZ's oxygen supply during EuO growth in extreme distillation by its oxygen ion conductivity: When the highly reactive Eu metal impinges the YSZ (001) surface, oxygen vacancies close to the YSZ's surface are created in favor of oxidizing  $Eu^0$  to  $Eu^{2+}$  or  $Eu^{3+}$ . As a direct consequence of the large oxygen ion conductivity, the vacancies can move freely through the entire bulk of the YSZ and do not accumulate at the interface. Furthermore, we found that less than 3 nm of EuO are formed on the YSZ (001) substrate w/o external O supply. For a substrate thickness of  $500 \mu m$  this means, that 6 uc EuO are located on top of almost  $10^6$  uc of YSZ. From this follows that only one of approximately 300 000 oxygen atoms is removed from the YSZ substrate, corresponding to a vacancy concentration of about 3.3 ppm.

As the YSZ's oxygen ion conductivity decreases with decreasing temperature, we also expect that the  $Eu^{3+}$  content of the film decreases at reduced growth temperatures. We performed the respective experiments for  $t_{Eu} = 60$  s at

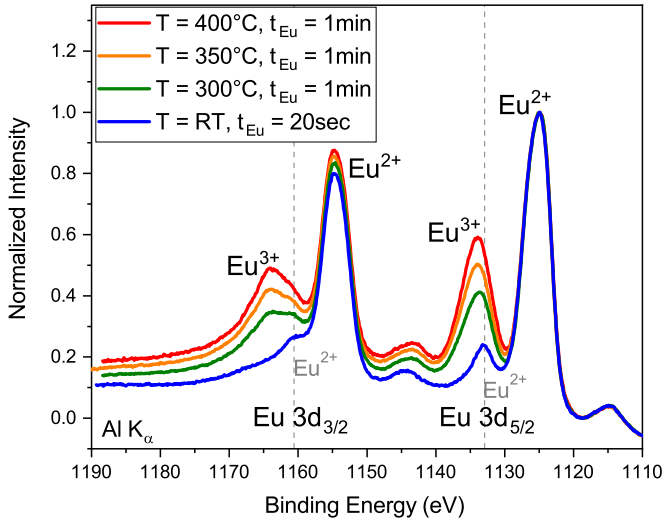


FIG. 7. Temperature dependence of extreme distillation growth. XPS spectra of the Eu  $3d_{5/2}$  core level of EuO/YSZ (001) films synthesized by supplying Eu metal for 1 min ( $T_S = 350^\circ\text{C}$ ,  $T_S = 300^\circ\text{C}$ ) and for 20 s ( $T = \text{RT}$ ). The  $\text{Eu}^{3+}$  content within the EuO film decreases with decreasing temperature, but is still significant at  $T_S = 300^\circ\text{C}$ . At RT, the EuO film might contain some  $\text{Eu}^0$  metal.

$T_S = 300^\circ\text{C}$  and  $T_S = 350^\circ\text{C}$ . At room temperature (RT), we deposited Eu metal for 20 s to be even more sensitive to the very first monolayer. The corresponding XPS spectra of the Eu  $3d_{5/2}$  core level are shown in Fig. 7 and exhibit a decrease of the  $\text{Eu}^{3+}$  feature ( $T_S = 350^\circ\text{C}$ : 28.5%  $\text{Eu}^{3+}$ ,  $T_S = 300^\circ\text{C}$ : 22%  $\text{Eu}^{3+}$ ), as expected for a decreased oxygen ion conductivity. However, it is still significant at  $T_S = 300^\circ\text{C}$ , which is close to the minimum temperature for the adsorption limited growth mode [16,17]. At room temperature, a small ratio of Eu metal is indicated by the unchanged position of the  $\text{Eu}^{2+}/\text{Eu}^0$  satellite of the Eu  $3d_{5/2}$  core level and the increased background at the high-energy side of the peak [21], indicating that (i) the oxygen supply from the substrate is lowered such that no  $\text{Eu}^{3+}$  is formed and (ii) no distillation takes place.

### C. Europium redox process

As shown before, we observed an initial interfacial overoxidation of the EuO/YSZ (001) films. Thus, for the ongoing growth, we have to consider the situation that Eu metal is deposited onto an oxygen-rich  $\text{EuO}_x$  film.

It is known that Eu metal and  $\text{Eu}_2\text{O}_3$  may undergo a disproportionation (redox) reaction resulting in stoichiometric EuO at a temperature of more than  $800^\circ\text{C}$  [29–31]. Furthermore, such a reaction has been used to synthesize EuO nanorods structures at reaction temperatures as low as  $450^\circ\text{C}$  [32–34]. It is thus necessary to investigate if such a process also takes place for thin films under common MBE growth conditions.

We experimentally studied this by depositing europium metal onto a fully oxidized ( $\text{Eu}_2\text{O}_3$ ) film. For this, we used the same  $\text{Eu}_2\text{O}_3$  sample from which we extracted the pure  $\text{Eu}^{3+}$  spectrum. Onto this film (green in Fig. 8), we deposited

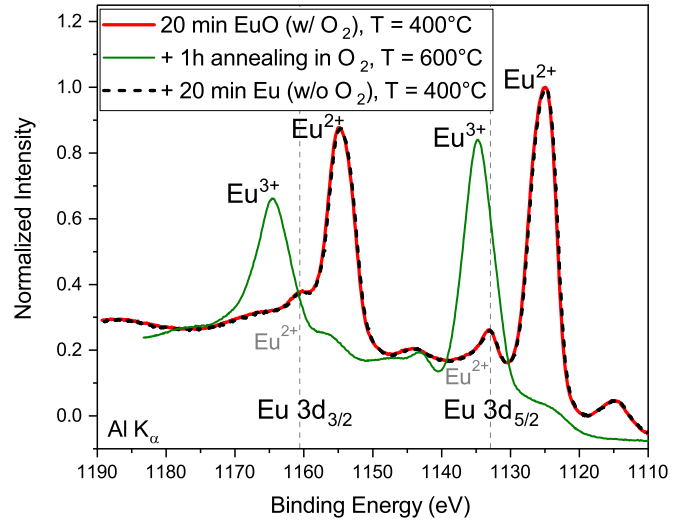
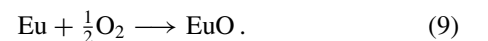
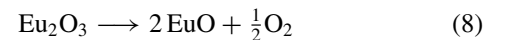


FIG. 8. XPS spectra of the Eu  $3d_{5/2}$  core level displaying the Eu-redox process. An initially stoichiometric film (red) is fully oxidized after  $\text{O}_2$  annealing at  $T_S = 600^\circ\text{C}$  (green) and became fully stoichiometric again after deposition Eu metal for another 20 min while the sample was kept at  $T_S = 400^\circ\text{C}$  (black dashed).

Eu metal w/o  $\text{O}_2$  supply at  $T_S = 400^\circ\text{C}$  for  $t_{\text{Eu}} = 20$  min. Surprisingly, this treatment results in fully stoichiometric EuO (black dashed in Fig. 8) again. The corresponding XPS spectrum perfectly matches the one of the initially synthesized stoichiometric EuO film (red in Fig. 8). We conclude that the experiment reveals a (reversible) Eu-redox (comproportionation) reaction,



The initially overoxidized film is reduced to EuO in favor of the oxidation of Eu to  $\text{EuO}$ , i.e.,



The thermodynamic description using the Gibbs free energy of formation  $\Delta G$  reads

$$\Delta G(\text{Eq. (8)}) = 2\Delta G(\text{EuO}) - \Delta G(\text{Eu}_2\text{O}_3) \quad (10)$$

$$\Delta G(\text{Eq. (9)}) = \Delta G(\text{EuO}), \quad (11)$$

and thus,

$$\Delta G(\text{Eq. (7)}) = \Delta G(\text{Eq. (10)}) + \Delta G(\text{Eq. (11)}) \quad (12)$$

$$= 3\Delta G(\text{EuO}) - \Delta G(\text{Eu}_2\text{O}_3). \quad (13)$$

From the thermodynamic point of view, the Eu-redox process will proceed if  $\Delta G(\text{Eu-redox}) = \Delta G(\text{Eq. (7)}) < 0$ . We calculate it from tabulated values at  $p = 1$  bar and  $T = 700$  K [35], close to our growth temperature of  $T_S = 400^\circ\text{C}$ . With  $\Delta G(\text{EuO}) = -508.8$  kJ/mol and  $\Delta G(\text{Eu}_2\text{O}_3) = -1430.6$  kJ/mol, we estimate

$$\Delta G(\text{Eu-redox}) = -95.8 \text{ kJ/mol}. \quad (14)$$

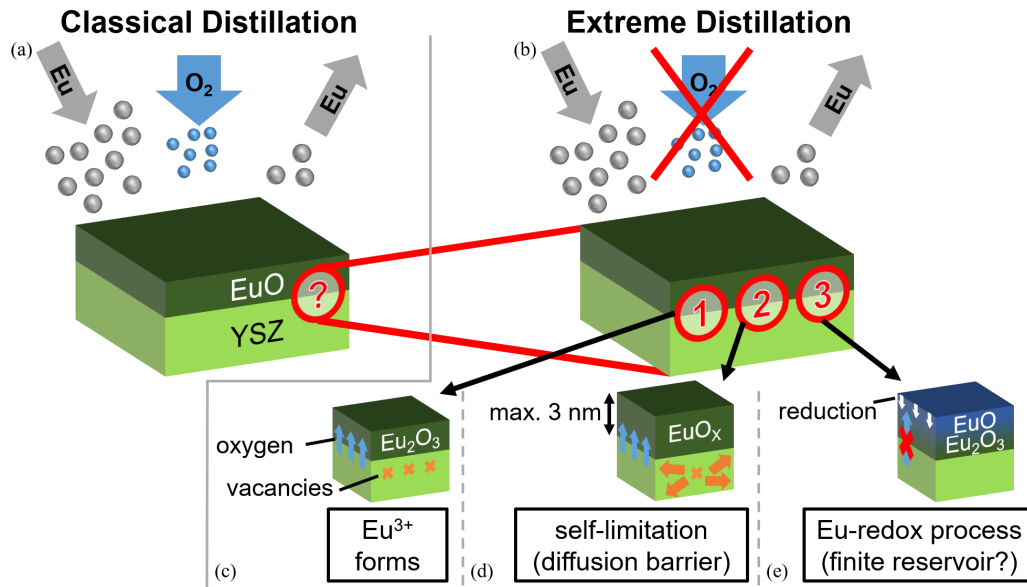


FIG. 9. Sketch of the three-process growth model for EuO/YSZ (001). While mainly hidden under (a) classical distillation conditions the individual processes are best observable under (b) extreme distillation conditions, i.e., the absence of externally supplied oxygen gas. (c) In process 1, a first oxygen-rich layer forms, which (d) acts as diffusion barrier and reduces the oxygen flux from the substrate towards the film surface, resulting in a self-limitation of the growth to a maximum EuO film thickness of about  $d_{\max} \approx 3$  nm. (e) Finally, an Eu-redox process is part of the growth process whenever the supply of Eu metal is larger than the oxygen supply at the surface (either as  $O_2$  gas or by diffusion).

Hence, the observation of an Eu-redox process is in line with thermodynamic considerations.

#### D. Three-process growth model of EuO/YSZ (001)

Based on the findings of the previous sections, we present a growth model for the formation of the very first monolayers of EuO on YSZ (001), sketched in Fig. 9. We propose three concurrent processes governing the growth in the case of extreme distillation, i.e., w/o external  $O_2$  supply, see Fig. 9(b). As shown in Sec. IV A, interfacial overoxidation of the  $EuO_x$  film takes place even if no oxygen is supplied externally. Thus, the first process is the formation of an oxygen-rich  $EuO_x$  layer at the YSZ (001) interface, Fig. 9(c). This layer (process 2, Fig. 9(d)) acts as a diffusion barrier in the following, as it reduces the oxygen diffusion from the substrate towards the EuO film's surface. As such, it causes a self-limitation of the EuO growth. We find that the thickness of the resulting EuO film is limited to  $d \leq 3$  nm at  $T_S = 400^\circ\text{C}$ . Within this process, the oxygen supply from the substrate may initially be still large enough to form further oxygen rich layers. However, the oxygen diffusion from the substrate towards the surface is further reduced by the increasing thickness of the  $EuO_x$  and it drops below the critical value for the formation of stoichiometric EuO. Possibly, the self-limitation is not only a consequence of the diffusion barrier but also of a finite oxygen reservoir, i.e., the oxygen vacancy concentration in the YSZ saturates.

Process 3, Fig. 9(e), is basically the Eu-redox process, as described in Sec. IV C. We studied this process in the extreme case where europium metal is deposited onto a fully oxidized film. However, we expect it to take place whenever an oxygen-rich film is exposed to adsorption limited growth

conditions, i.e., when the supply of europium metal is larger than that of oxygen diffused from the substrate towards the film surface. This situation occurs once the oxygen diffusion from the substrate towards the film's surface is reduced below the critical value for the formation of stoichiometric EuO (process 2). As a consequence, the oxygen-rich region formed as described in processes 1 and 2 may shrink again.

These three processes likely proceed concurrently and are generally expected to be present not only under oxygen-free growth conditions (extreme distillation), but also if oxygen gas is supplied externally. However, once the system reaches its equilibrium, i.e., no oxygen is supplied at the film surface by the sample itself, synthesis is only possible w/externally supplied oxygen, see Fig. 9(a).

#### V. DISCUSSION

The observation of interfacial overoxidation of EuO/YSZ (001) at a deposition temperature of  $T_S = 400^\circ\text{C}$  is in contrast to the current status of understanding, which claims a stoichiometric growth from the first monolayer on [15]. However, we investigated much thinner films compared, e.g., to Sutarto *et al.* [15]. Therefore, we are able to reveal the growth and redox processes at the very first monolayers.

Formation of  $Eu^{3+}$  by oxygen originating from the YSZ substrate can not be explained in terms of bulk thermodynamics. We discussed that the growth process is operated under highly nonequilibrium conditions and, hence, they are not covered by bulk thermodynamics. We further approximated the average reduction of the YSZ substrate to be proportional to a release of approximately 3.3 ppm of its oxygen. This shows that within certain limits, also processes beyond

thermodynamics, i.e., the formation of oxygen vacancies  $V_{\text{O}}^{\bullet\bullet}$  in the YSZ substrate, have to be taken into account for EuO thin film synthesis. Besides kinetics of the oxygen ion reservoir and the Eu atoms at the surface as well as thermodynamics of the interface reactions as discussed for EuO/SrTiO<sub>3</sub> [21], this has to be considered as a fourth factor for oxygen-free growth of EuO.

The importance of the kinetics of the oxygen reservoir is pronounced by the finding that even at  $T_S = 300^\circ\text{C}$  a significant ratio of  $\text{Eu}^{3+}$  (22%) is present in the ultrathin ( $t_{\text{Eu}} = 1$  min) film. As this temperature is known to be close to the critical temperature for remaining in the adsorption limited growth mode [16,17], we conclude that very likely interfacial overoxidation of EuO/YSZ (001) is unavoidable within the adsorption limited growth mode, at least in a well-established range of MBE growth conditions.

We found an Eu-redox process taking place when Eu metal is deposited onto an  $\text{Eu}^{3+}$ -rich film. This is in general the case whenever EuO synthesis is supposed to be performed in the adsorption limited growth mode and initial interfacial overoxidation takes place, as for EuO/YSZ (001). Likely, the redox process is relevant for growth on other oxidic substrates and will be subject to future studies. We expect an increasing importance if the substrate's oxygen supply is strong and allows for the formation of  $\text{Eu}^{3+}$  in the beginning of the growth process but the reservoir is finite. In this case, the overoxidized state can not be maintained by a constant oxygen supply.

The presented three-process growth model covers, e.g., the description based on a Mott-Cabrera-like process for EuO/SrTiO<sub>3</sub> [21] and is, thus, not limited to EuO/YSZ (001). So far, however, the growth model is just supposed to be regarded as a basic guideline for the understanding of

EuO synthesis on oxidic substrates and refinements will be necessary. In order to properly place the Eu-redox process within the model, further studies, also using other oxidic substrates, are required.

## VI. SUMMARY

In summary, by an XPS study, we revealed novel aspects of the synthesis of atomically thin EuO on its model substrate YSZ. We found that EuO growth on YSZ is not as ideal as described so far [15]: Initial overoxidation of the overlayer was detected at  $T_S = 400^\circ\text{C}$  as well as at lower growth temperatures. The latter indicates that interfacial overoxidation is unavoidable within a certain and common range of growth parameters. For YSZ as a substrate, this process is beyond a purely thermodynamic description. We assume that besides the relatively high (compared to, e.g., LaAlO<sub>3</sub> [28]) oxygen ion conductivity of the substrate, also its affinity to the formation of oxygen vacancies is an important factor for the oxygen supply by the substrate.

We found a reversible Eu-redox process that is relevant in the growth process of EuO ultrathin films, which is intriguing to be considered in future studies on EuO growth on oxidic substrates. We derived a three-process growth model as a new guideline for the synthesis of EuO on YSZ in particular and on oxidic substrates in general.

## ACKNOWLEDGMENTS

We would like to thank Patrick Lömker and David N. Mueller for insightful discussions. This work was supported by the Deutsche Forschungsgemeinschaft through the International Collaborative Research Center TRR160 (Project C9).

- 
- [1] M. Lorenz, M. S. Ramachandra Rao, T. Venkatesan, E. Fortunato, P. Barquinha, R. Branquinho, D. Salgueiro, R. Martins, E. Carlos, A. Liu, F. K. Shan, M. Grundmann, H. Boschker, J. Mukherjee, M. Priyadarshini *et al.*, The 2016 oxide electronic materials and oxide interfaces roadmap, *J. Phys. D* **49**, 433001 (2016).
- [2] M. Müller, P. Lömker, P. Rosenberger, M. Hussein Hamed, D. N. Mueller, R. A. Heinen, T. Szyjka, and L. Baumgarten, Hard x-ray photoelectron spectroscopy of tunable oxide interfaces, *J. Vac. Sci. Technol. A* **40**, 013215 (2022).
- [3] A. Ohtomo and H. Y. Hwang, A high-mobility electron gas at the LaAlO<sub>3</sub>/SrTiO<sub>3</sub> heterointerface, *Nature (London)* **427**, 423 (2004).
- [4] C. W. Schneider, M. Esposito, I. Marozau, K. Conder, M. Doebeli, Y. Hu, M. Mallepell, A. Wokaun, and T. Lippert, The origin of oxygen in oxide thin films: Role of the substrate, *Appl. Phys. Lett.* **97**, 192107 (2010).
- [5] C. W. Schneider, M. Döbeli, C. Richter, and T. Lippert, Oxygen diffusion in oxide thin films grown on SrTiO<sub>3</sub>, *Phys. Rev. Mater.* **3**, 123401 (2019).
- [6] M. H. Hamed, R. A. Hinz, P. Lömker, M. Wilhelm, A. Gloskovskii, P. Bencok, C. Schmitz-Antoniak, H. Elnaggar, C. M. Schneider, and M. Müller, Tunable magnetic phases at Fe<sub>3</sub>O<sub>4</sub>/SrTiO<sub>3</sub> oxide interfaces, *ACS Appl. Mater. Interfaces* **11**, 7576 (2019).
- [7] M. H. Hamed, D. N. Mueller, and M. Müller, Thermal phase design of ultrathin magnetic iron oxide films: from Fe<sub>3</sub>O<sub>4</sub> to  $\gamma$ -Fe<sub>2</sub>O<sub>3</sub> and FeO, *J. Mater. Chem. C* **8**, 1335 (2020).
- [8] M. H. Hamed, D. N. Mueller, and M. Müller, Active participation of "inert" YSZ substrates on interface formation in Fe<sub>3</sub>O<sub>4</sub>/YSZ heterostructures, *Appl. Surf. Sci. Adv.* **6**, 100132 (2021).
- [9] P. Rosenberger, M. Opel, S. Geprägs, H. Huebl, R. Gross, M. Müller, and M. Althammer, Quantifying the spin mixing conductance of EuO/W heterostructures by spin Hall magnetoresistance experiments, *Appl. Phys. Lett.* **118**, 192401 (2021).
- [10] G. M. Prinz, T. Gerber, A. Lorke, and M. Müller, Quantum confinement in EuO heterostructures, *Appl. Phys. Lett.* **109**, 202401 (2016).
- [11] P. Lömker, T. C. Rödel, T. Gerber, F. Fortuna, E. Frantzeskakis, P. Le Fèvre, F. Bertran, M. Müller, and A. F. Santander-Syro, Two-dimensional electron system at the magnetically tunable EuO/SrTiO<sub>3</sub> interface, *Phys. Rev. Mater.* **1**, 062001(R) (2017).



- [12] R. P. Ingel and D. Lewis III, Lattice parameters and density for  $Y_2O_3$ -stabilized  $ZrO_2$ , *J. Am. Ceram. Soc.* **69**, 325 (1986).
- [13] R. C. Rau, X-ray crystallographic studies of Europium oxides and hydroxides, Tech. Rep. CONF-20-18; TM-63-2-8 (General Electric Co. Advanced Technology Services, Cincinnati, 1962)
- [14] T. Gerber, P. Lömker, B. Zijlstra, C. Besson, D. N. Mueller, W. Zander, J. Schubert, M. Gorgoi, and M. Müller, Thermodynamic stability and control of oxygen reactivity at functional oxide interfaces: EuO on ITO, *J. Mater. Chem. C* **4**, 1813 (2016).
- [15] R. Sutarto, S. G. Altendorf, B. Coloru, M. Moretti Sala, T. Haupricht, C. F. Chang, Z. Hu, C. Schüßler-Langeheine, N. Hollmann, H. Kierspel, H. H. Hsieh, H.-J. Lin, C. T. Chen, and L. H. Tjeng, Epitaxial and layer-by-layer growth of EuO thin films on yttria-stabilized cubic zirconia (001) using MBE distillation, *Phys. Rev. B* **79**, 205318 (2009).
- [16] S. G. Altendorf, A. Efimenko, V. Oliana, H. Kierspel, A. D. Rata, and L. H. Tjeng, Oxygen off-stoichiometry and phase separation in EuO thin films, *Phys. Rev. B* **84**, 155442 (2011).
- [17] P. Steeneken, Ph.D. thesis, University of Groningen, 2002.
- [18] C. Caspers, A. Gloskovskii, W. Drube, C. M. Schneider, and M. Müller, "Conductive" yttria-stabilized zirconia as an epitaxial template for oxide heterostructures, *J. Appl. Phys.* **115**, 17C111 (2014).
- [19] I. Moder, G. Garcia, J. Santiso, J. S. Moodera, G. X. Miao, A. F. Lopeandía, and J. Rodríguez-Viejo, Reduction of the deposition temperature of high quality EuO films on Yttria Stabilized Zirconia by incorporating an MgO buffer layer, *Thin Solid Films* **531**, 466 (2013).
- [20] A. Schmehl, V. Vaithyanathan, A. Herrnberger, S. Thiel, C. Richter, M. Liberati, T. Heeg, M. Röckerath, L. F. Kourkoutis, S. Mühlbauer, P. Böni, D. A. Muller, Y. Barash, J. Schubert, Y. Idzerda, J. Mannhart, and D. G. Schlom, Epitaxial integration of the highly spin-polarized ferromagnetic semiconductor EuO with silicon and GaN, *Nature Mater.* **6**, 882 (2007).
- [21] P. Lömker and M. Müller, Redox-controlled epitaxy and magnetism of oxide heterointerfaces: EuO/SrTiO<sub>3</sub>, *Phys. Rev. Mater.* **3**, 061401(R) (2019).
- [22] C. Caspers, Ph.D. thesis, Universität Duisburg, 2013.
- [23] E.-J. Cho, S.-J. Oh, S. Imada, S. Suga, T. Suzuki, and T. Kasuya, Origin of the high-binding-energy structure in the 3d core-level spectra of divalent Eu compounds, *Phys. Rev. B* **51**, 10146 (1995).
- [24] A. Jablonski and C. J. Powell, Effective attenuation lengths for photoelectrons emitted by high-energy laboratory X-ray sources, *J. Electron Spectrosc. Relat. Phenom.* **199**, 27 (2015).
- [25] W. S. M. Werner, W. Smekal, and C. J. Powell, *NIST Database for the Simulation of Electron Spectra for Surface Analysis, Version 2.0* (National Institute of Standards and Technology, Gaithersburg, 2014).
- [26] F. A. Kröger and H. J. Vink, *Relations between the Concentrations of Imperfections in Crystalline Solids* (Academic Press, New York, 1956), pp. 307–435.
- [27] S. J. Skinner and J. A. Kilner, Oxygen ion conductors, *Mater. Today* **6**, 30 (2003).
- [28] T. L. Nguyen, M. Dokiya, S. Wang, H. Tagawa, and T. Hashimoto, The effect of oxygen vacancy on the oxide ion mobility in LaAlO<sub>3</sub>-based oxides, *Solid State Ionics* **130**, 229 (2000).
- [29] M. W. Shafer, Preparation and Crystal Chemistry of Divalent Europium Compounds, *J. Appl. Phys.* **36**, 1145 (1965).
- [30] M. Shafer, J. Torrance, and T. Penney, Relationship of crystal growth parameters to the stoichiometry of EuO as determined by I.R. and conductivity measurements, *J. Phys. Chem. Solids* **33**, 2251 (1972).
- [31] A. Borukhovich and A. Troshin, *Europium Monoxide: Semiconductor and Ferromagnet for Spintronics*, Springer Series in Materials Science (Springer International Publishing, Berlin, 2018).
- [32] M. J. Bierman, K. M. Van Heuvelen, D. Schmeißer, T. C. Brunold, and S. Jin, Ferromagnetic Semiconducting EuO Nanorods, *Adv. Mater.* **19**, 2677 (2007).
- [33] B. Trepka, P. Erler, S. Selzer, T. Kollek, K. Boldt, M. Fonin, U. Nowak, D. Wolf, A. Lubk, and S. Polarz, Nanomorphology Effects in Semiconductors with Native Ferromagnetism: Hierarchical Europium (II) Oxide Tubes Prepared via a Topotactic Nanostructure Transition, *Adv. Mater.* **30**, 1703612 (2018).
- [34] B. Trepka, J. Stiegeler, I. Wimmer, M. Fonin, and S. Polarz, EurOgels: A ferromagnetic semiconductor with a porous structure prepared via the assembly of hybrid nanorods, *Nanoscale* **10**, 19272 (2018).
- [35] R. A. Robie, B. S. Hemingway, and J. R. Fisher, *Thermodynamic properties of minerals and related substances at 298.15 K and 1 bar (105 pascals) pressure and at higher temperatures*, Tech. Rep. 1452 (U.S. Geological Survey, Washington D.C., 1978).